minerals

Article

Geochronology and Petrogenesis of the Early Paleozoic Jilongjie Granites in the Central South China Block: Implication for Post-Kinematic Lithospheric Delamination

Haiyang He [1,2,3], Tingting Wang [1], Qinglin Sui [1], Xianzhe Duan [1], Xuan Ren [1], Danping Hou [1], Yanshi Xie [1], Shan Liu [1], Peng Feng [1], Huanbao Zhang [1,*] and Liang Chen [1,2,*]

[1] School of Resource & Environment and Safety Engineering, University of South China, Hengyang 421001, China
[2] State Key Laboratory of Nuclear Resources and Environment, East China University of Technology, Nanchang 330013, China
[3] Hunan Key Laboratory of Rare Metal Minerals Exploitation and Geological Disposal of Wastes, University of South China, Hengyang 421001, China
* Correspondence: 2019000068@usc.edu.cn (H.Z.); 2010000502@usc.edu.cn (L.C.)

Abstract: Controversy over the geodynamic interpretation of the early Paleozoic granites in the South China Block constrains understanding of tectonic–magmatic evolution. In this paper, we present zircon U-Pb age, Hf isotope, and major and trace element data of the early Paleozoic granites in the Jilongjie region, south-central Hunan Province. A sample that yielded a weighted average $^{206}Pb/^{238}U$ age of 425 ± 3 Ma falls into the post-collisional granite field in the classification discriminant of magmatic rocks. Geochemical features indicate that the Jilongjie pluton is a shoshonitic metaluminous rock. The Jilongjie pluton's chondrite-normalized rare earth element patterns exhibit a slight enrichment of light rare earth elements (LREEs) relative to heavy rare earth elements (HREEs) with $(La/Yb)_N$ ratios of 15.1–23.7 and weak Eu anomalies (Eu/Eu* = 0.68–0.78). Zircon Hf isotope results show $\varepsilon_{Hf}(t)$ ranging from −9.94 to −0.69. Jilongjie granite's parent magma originated from a mixing of crust-derived felsic and mantle-derived mafic magmas, which then underwent fractional crystallization during its ascent. Jilongjie granite was generated through a post-collisional extensional setting associated with delamination of the thickened lithosphere.

Keywords: geochronology; petrogenesis; early Paleozoic; Jielongjie pluton; South China Block

check for updates

Citation: He, H.; Wang, T.; Sui, Q.; Duan, X.; Ren, X.; Hou, D.; Xie, Y.; Liu, S.; Feng, P.; Zhang, H.; et al. Geochronology and Petrogenesis of the Early Paleozoic Jilongjie Granites in the Central South China Block: Implication for Post-Kinematic Lithospheric Delamination. *Minerals* **2023**, *13*, 734. https://doi.org/10.3390/min13060734

Academic Editors: Alexey V. Ivanov and Clemente Recio

Received: 12 February 2023
Revised: 24 May 2023
Accepted: 25 May 2023
Published: 29 May 2023

1. Introduction

The South China Block (SCB) was formed by the amalgamation of the Cathaysia Block in the southeast and the Yangtze Block in the northwest during the Neoproterozoic [1–5]. There is a significant amount of granite in the South China Block, which is generally considered one of the largest granite provinces in the world [6,7]. These granites are considered to have responded to the Caledonian, Indosinian, and Yanshanian tectonic events in the South China Block [7–20]. Caledonian massive granitic intrusions outcrop to the east of the Anhua–Luocheng Fault zone as batholiths and laccoliths, and are important components of the Phanerozoic granites in the eastern South China Block (Figure 1).

In recent years, many studies have been carried out on Indosinian and Yanshanian granites in the South China Block; Yanshanian granites are closely related to large-scale mineralization [21–25]. However, the petrogenesis and tectonic setting of Caledonian granites are still controversial (Table 1), with different viewpoints on tectonic settings, such as continental margin arc, oceanic–continental subduction, continental collision, and intracontinental orogeny.

In this paper, we present zircon U-Pb dating, Hf isotope results, and whole-rock geochemical data for the early Paleozoic granites in the south-central Hunan, central

South China Block, which have previously received much attention. In-depth study of the petrogenesis and tectonic setting provides information to further understanding of the SCB's early Paleozoic tectonic–magmatic evolution.

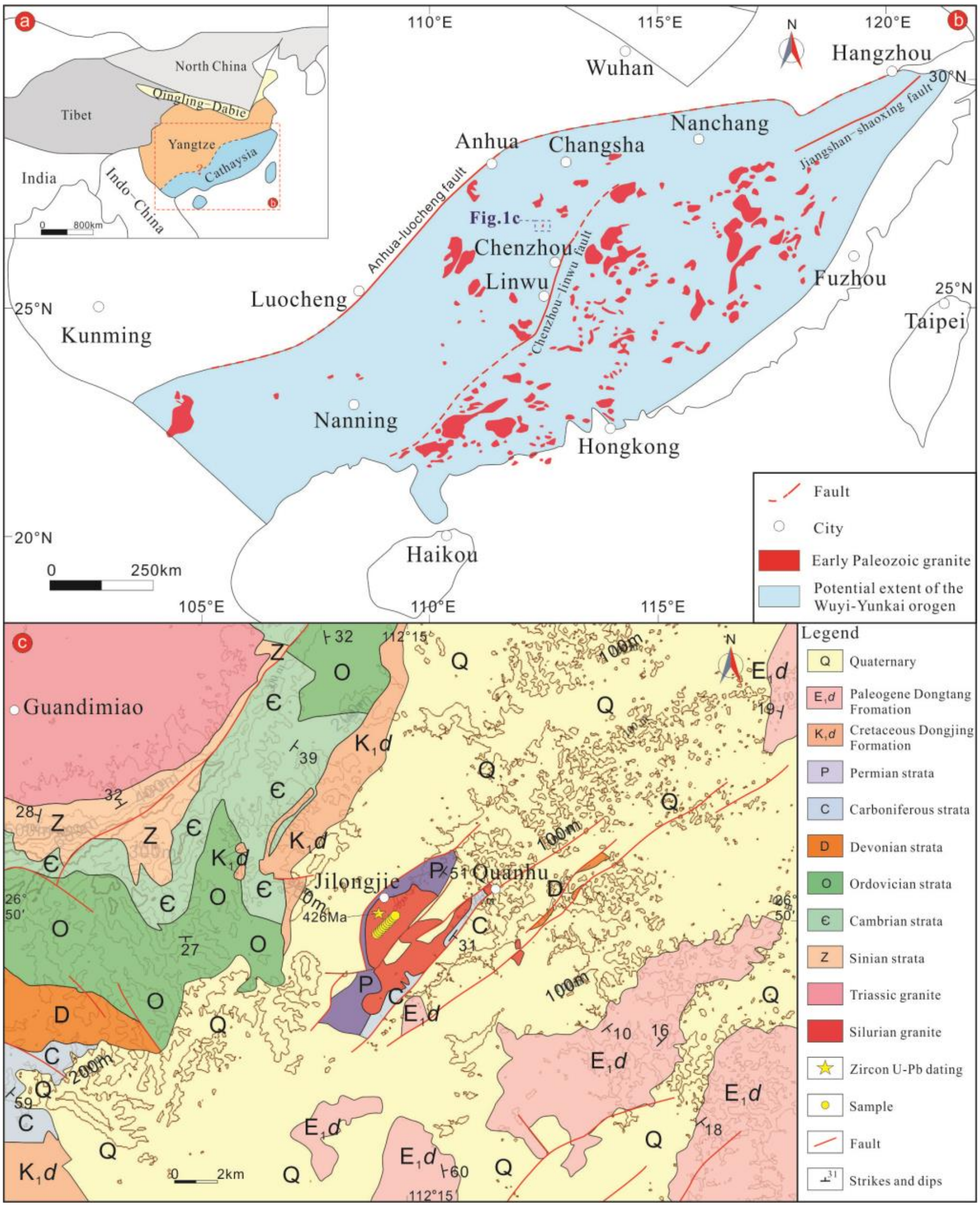

Figure 1. (**a**) Geotectonic map of China and its adjacent areas; (**b**) simplified geological map showing the distribution of the Early Middle Paleozoic granites in the eastern SBC (modified from Li, et al. [26] and Zhao, et al. [27]); (**c**) geological map of the Jilongjie area. Part of the data sources are shown in Table 1.

Table 1. Summary ages of the Early Middle Paleozoic rocks in SCB.

Number	Locality	Lithology	Dating Method	Age (Ma)	Literature
1	Tanghu	Granite	Zircon U-Pb dating	433 ± 2	[28]
	Wangyangshan	Granite	Zircon U-Pb dating	434	
2	Guidong	Granodiorite	Zircon U-Pb dating	425.5 ± 1.7	[29]
	Zhaiqian	Granite	Zircon U-Pb dating	430.7 ± 1.9	
3	Napeng	Granite	Zircon U-Pb dating	418 ± 12	[30]
4	Song Chay	Granite	Zircon U-Pb dating	428 ± 5	[31]
5	Zhuguang	Granite	Zircon U-Pb dating	446.7 ± 6.3; 424.6 ± 3.7	[32]
6	Songwang	Foliated granite	Zircon U-Pb dating	440.7 ± 5.6	[7]
	Dagu	Granitic gneiss		421.9 ± 9.8	
	Yuntan	Biotite orthogneiss		427.1 ± 4.2	
	Chidong	Biotite paragneiss		423.0 ± 7.0	
	Hebapu	Granitic gneiss		429.6 ± 5.2	
7	Weipu	Granite	Zircon U-Pb dating	427.4 ± 4.0	[33]
8	Northwestern Fujian	Granite	Zircon U-Pb dating	437 ± 5; 437 ± 4; 440 ± 5; 441 ± 4	[34]
9	Tianjingping	Granodiorite	Zircon U-Pb dating	447 ± 2	[35]
10	Sibao	Granite	Shrimp U-Pb zircon	432	[26]
	Weipu			433	
11	Yunkai	Granite; gneissic granite	Zircon U-Pb dating	430 ± 10; 443 ± 4; 437 ± 5	[36]
12	Wugong domain	Gneissoid granite; orthogneiss; migmatite	Zircon U-Pb dating	455 ± 8; 455 ± 9; 456 ± 5; 443 ± 5; 424 ± 6; 452 ± 4	[37]
	Northern Wuyi domain	Genissoid granite; orthogneiss; migmatite		410 ± 10; 427 ± 15; 430 ± 9; 457 ± 6	
	Southern Wuyi domain	Genissoid granite; orthogneiss		430 ± 6; 438 ± 3; 432 ± 6; 427 ± 4; 426 ± 6; 426 ± 8; 437 ± 3; 430 ± 6	
	Yunkai domain	Orthogneiss; gneissoid granite; leucosome in migmatite; paragneiss		450 ± 8; 449 ± 5; 443 ± 7; 415 ± 7; 435 ± 8; 452 ± 6	
13	Wuping	Gneissic granite		496 ± 4; 494 ± 6	[38]
14	Le'an	Biotite monzogranite	Zircon U-Pb dating	429 ± 2	[39]
	Zhangjiafang	Biotite monzogranite		440 ± 2	
	Shuangzhuang	Monzogranite; biotite monzogranite		424 ± 4; 441 ± 3	
	Pengongmiao	Monzogranite		405 ± 3	
	Wanyangshan	Monzogranite		433 ± 4	
	Tanghu	Monzogranite		454 ± 2	
	Banshanpu	Monzogranite		418 ± 2	
	Hongxiaqiao	Granodiorite		432 ± 6	
	Miaoershan	Monzogranite		400 ± 4; 415 ± 2	
	Haiyangshan	Biotite monzogranite		429 ± 11	
	Fengdingshan	Granodiorite		402 ± 2	

Table 1. *Cont.*

Number	Locality	Lithology	Dating Method	Age (Ma)	Literature
15	Xuefengshan Beltt	Granite	Zircon U-Pb dating	428 ± 4; 438 ± 3; 437 ± 4; 411 ± 4; 412 ± 4; 424 ± 3	[40]
16	Taishan	Granite	Zircon U-Pb dating	436 ± 3; 436 ± 3; 436 ± 4; 436 ± 6;	[41]
17	Yuechenling Miaoershan	Granite	Zircon U-Pb dating	435 ± 4; 427 ± 3; 417 ± 6 404 ± 4	[27]
18	Northern Guangdong	Basalt; andesite; dacite, ignimbrite	Zircon U-Pb dating; Shrimp U-Pb dating	435 ± 6; 435 ± 6	[42]
19	Yunkai	Charnockite	Zircon U-Pb dating	439 ± 2; 439 ± 4	[43]
20	Doulong	Granite	Zircon U-Pb dating	429 ± 3; 430 ± 3; 430 ± 2; 430 ± 2	[44]
21	Shangmushui	Granodiorite	Zircon U-Pb dating	444 ± 4	[45]
22	Wanyangshan	Tonalite; granodiorite; monzonitic granite	Zircon U-Pb dating	438 ± 3; 426 ± 3	[46]
23	Daning	Granite	SHRIMP	419.1 ± 6.4	[47]

2. Geological Setting and Petrography

The SCB consists of the Cathaysia Block in the southeast and the Yangtze Block in the northwest. The northeasterly trending Jiangshan–Shaoxing Fault is the present boundary between the Cathaysia Block and the Yangtze Block [25,39,48]. However, the southwestern extension is uncertain due to intensive younger tectonic modification and poor exposure.

The Cathaysia basement is considered to be predominantly composed of gneiss, schist, migmatite, amphibolite, and pyroclastic rocks from the Mesoproterozoic and Paleoproterozoic ages [14,49–51]. The Precambrian Cathaysia Block basement can be divided into the Nanling–Yunkai terrane in the southwest and the Wuyishan terrane in the northeast [52]. The oldest basement rocks in the Cathaysia Block are amphibolites (~1.80 Ga) distributed on the Wuyishan terrane [53]. Moreover, minor Mesoproterozoic granite (~1.43 Ga) was identified on Hainan Island in the south [54]. Recently, some Neoproterozoic mafic rocks were identified in the Cathaysian block [55]. The basement of the Yangtze Block is mainly composed of Proterozoic rocks, with minor Archean rocks, such as Kongling complex, dating to ca. 3.2 Ga [56–59]. Moreover, Neoproterozoic volcanic rocks appear around the Yangtze Block.

Samples for this study were collected in Jilongjie Town, 30 km southwest of Hengyang City, Hunan Province (N 26°50′17.81″; E 112°15′10.21″). The plutonic rock area is approximately 25 km^2; host rocks are quartz sandstone and siltstone of the Permian Yangping and Leping Formation, as well as Carboniferous dolomite and dolomitic limestone. Plutonic rocks are in nonconformity contact with host rocks (Figure 2a). Exposed rock units in the study area also include Sinian slate, dolomite and limestone, Cambrian slate and phyllite, Ordovician phyllite and limestone, Devonian limestone, dolomite and mudstone, Carboniferous sandstone and siltstone, Cretaceous Dongjing Formation sandstone and conglomerate, Paleogene Dongtang Formation sandstone and sandy mudstone, and Quaternary sandy clay and sandy soil (Figure 1c).

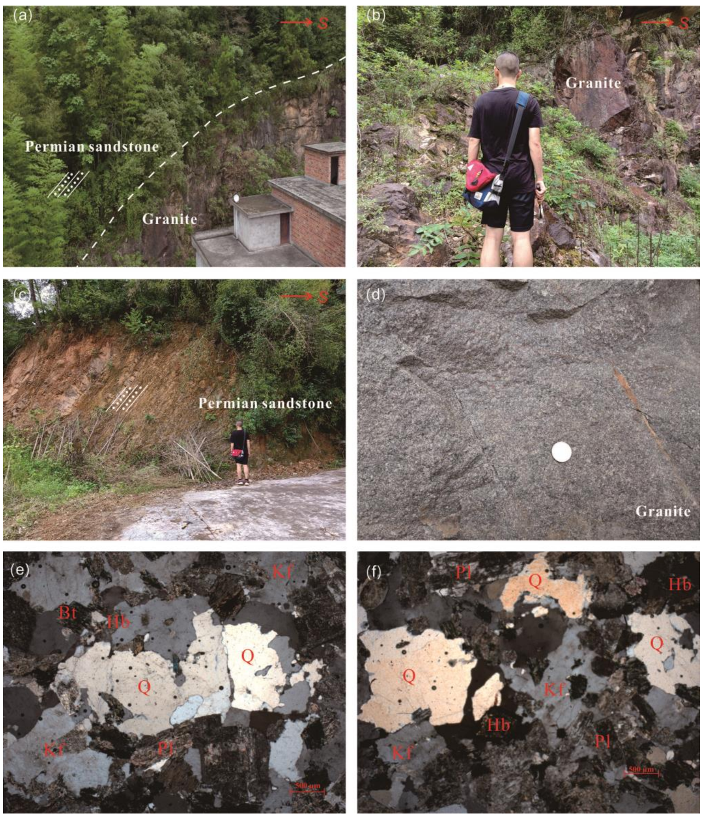

Figure 2. (**a**) Field contact relationship between rocks; (**b**) field photo of Jilongjie granite; (**c**) field photo of Permian sandstone; (**d**) hand specimen photo of Jilongjie granite; (**e**,**f**) photomicrographs of Jilongjie granite. Q—quartz; Kf—potassium feldspar; Pl—plagioclase; Bt—biotite; Hb—hornblende.

Jilongjie plutonic rocks are uniform in structure; their main minerals are K-feldspar (35%~40%), plagioclase (25%~30%), quartz (20%~30%), biotite (6%~10%), and amphibole (2%~4%); their accessory minerals include titanite, magnetite, and zircon (Figure 2e,f). Plagioclase occurs mainly as euhedral plate-like crystals, with albite twining; K-feldspar and quartz are anhedral (Figure 2e,f).

3. Analytical Methods

Zircon U-Pb dating, major and trace element analyses of whole rock, and zircon Hf isotopic analyses were conducted at the Wuhan SampleSolution Analytical Technology Co., Ltd., Wuhan, China. Zircon U-Pb dating analysis was conducted using laser ablation inductively coupled plasma mass spectrometry (LA-ICP-MS). Detailed operating conditions for the LA system and ICP-MS instrument and data reduction were the same as described in [60]. Ion-signal intensities were acquired using an Agilent 7700e (Agilent Technology, Tokyo, Japan). In this study, the spot size was set to 32 μm and the laser frequency was set to 5 Hz. U-Pb dating and trace element calibration used zircon 91500 and glass NIST610 (Wuhan SampleSolution Analytical Technology Co., Ltd., Wuhan, China) as external standards, respectively. Off-line selection and integration of background and analyzed signals, time-drift correction, and quantitative calibration for trace element analysis and U-Pb dating were completed using ICPMSDataCal 12.2, an Excel-based software [61]. Concordia diagrams and weighted mean calculations of zircon samples were conducted using the Isoplot/Ex (version 3.0) program [62].

Major and trace element analyses of whole rock were performed using X-ray fluorescence (XRF, Rigaku, Japan) and ICP-MS (Agilent 7700e). Analytical uncertainties for major elements were generally <1 wt.%. Analytical results for AGV-2, BHVO-2, BCR-2, and RGM-2 international standards indicate that accuracies were better than 5% for most elements. The analytical procedure details were as described by Liu, et al. [63].

Hafnium isotope ratio analysis experiments were conducted in situ using a Neptune Plus multicollector (MC) ICP-MS (Thermo Fisher Scientific, Germany) in combination with a Geolas HD excimer ArF laser ablation system (Coherent, Göttingen, Germany). This laser ablation system includes a "wire" signal smoothing device that produces smooth signals even at very low laser repetition rates (as low as 1 Hz) [64]. Helium was the carrier gas within the ablation cell, and was merged with argon (makeup gas) after the ablation cell. Small amounts of nitrogen were added to the argon makeup gas flow to improve its sensitivity to Hf isotopes [65]. Compared to the standard arrangement, the addition of nitrogen in combination with the newly designed X skimmer cone and Jet sample cone in Neptune Plus improved the signal intensities of Hf, Yb, and Lu by factors of 5.3, 4.0, and 2.4, respectively. Detailed operating conditions for the laser ablation system, the MC-ICP-MS instrument, and the analytical method were the same as those described by Hu, et al. [66].

4. Results

4.1. Zircon U-Pb Geochronological Results

In this study, seventeen zircon grains in a sample (JL-U) from the Jilongjie pluton were selected for LA-ICP-MS dating. Zircon U-Pb data are listed in Table 2, and the concordia diagram is shown in Figure 3a. These zircon grains were euhedral, gray-white, or colorless. The crystals were elongated with lengths ranging from 120 to 280 μm and aspect ratios from 2:1 to 5:1. In cathodoluminescence, zircon crystals showed a clear and dense ring structure, indicating magmatic origin (Figure 3a). Zircon trace element data showed high Th/U values, which also indicate a magmatic crystallization origin [67]. Zircon trace element contents are listed in Table 3, and the chondrite-normalized REE diagram is shown in Figure 3b. Zircon crystals had similar characteristics to typical magmatic zircons [67], such as positive Ce and negative Eu anomalies, and HREE enrichment relative to LREE (Figure 3b).

Table 2. LA-ICP-MS results of zircon from the Jilongjie pluton.

Samples and Anal. NO.	Th (ppm)	U (ppm)	Th/U Ratio	Isotopic Ratios (±1σ)						Ages (±1σ Ma)						Concordance
				$^{207}Pb/^{206}Pb$		$^{207}Pb/^{235}U$		$^{206}Pb/^{238}U$		$^{207}Pb/^{206}Pb$		$^{207}Pb/^{235}U$		$^{206}Pb/^{238}U$		
1. JL-U-01	838	1047	0.80	0.0599	0.0013	0.5609	0.0110	0.0679	0.0006	611	51	452	7	423	4	93%
2. JL-U-02	535	745	0.72	0.0602	0.0013	0.5762	0.0128	0.0692	0.0006	613	46	462	8	431	4	93%
3. JL-U-03	963	1035	0.93	0.0572	0.0013	0.5332	0.0112	0.0676	0.0007	498	45	434	7	421	4	97%
4. JL-U-04	1019	1029	0.99	0.0615	0.0012	0.5906	0.0119	0.0693	0.0007	657	44	471	8	432	4	91%
5. JL-U-05	628	867	0.72	0.0612	0.0013	0.5828	0.0119	0.0687	0.0005	656	38	466	8	428	3	91%
6. JL-U-06	575	772	0.75	0.0593	0.0012	0.5589	0.0107	0.0680	0.0005	589	10	451	7	424	3	93%
7. JL-U-07	705	908	0.78	0.0520	0.0011	0.4865	0.0100	0.0679	0.0007	283	48	403	7	423	4	94%
8. JL-U-08	824	973	0.85	0.0576	0.0012	0.5487	0.0115	0.0688	0.0006	522	44	444	8	429	3	96%
9. JL-U-09	648	926	0.70	0.0566	0.0012	0.5334	0.0110	0.0681	0.0005	476	46	434	7	425	3	97%
10. JL-U-10	1465	1032	1.42	0.0565	0.0013	0.5360	0.0120	0.0688	0.0006	478	52	436	8	429	4	98%
11. JL-U-11	584	1001	0.58	0.0578	0.0012	0.5395	0.0108	0.0673	0.0005	524	44	438	7	420	3	95%
12. JL-U-12	541	883	0.61	0.0570	0.0012	0.5332	0.0109	0.0676	0.0005	494	42	434	7	422	3	97%
13. JL-U-13	710	951	0.75	0.0620	0.0012	0.5737	0.0106	0.0668	0.0005	676	43	460	7	417	3	90%
14. JL-U-14	666	968	0.69	0.0579	0.0012	0.5563	0.0113	0.0693	0.0005	528	46	449	7	432	3	96%
15. JL-U-15	610	859	0.71	0.0567	0.0013	0.5344	0.0115	0.0679	0.0005	480	48	435	8	424	3	97%
16. JL-U-16	691	939	0.74	0.0565	0.0012	0.5409	0.0110	0.0691	0.0005	472	44	439	7	431	3	98%
17. JL-U-17	1048	960	1.09	0.0605	0.0013	0.5807	0.0124	0.0693	0.0006	620	46	465	8	432	3	92%

Table 3. Trace element (ppm) data of zircon from the Jilongjie pluton.

Samples	La	Ce	Pr	Nd	Sm	Eu	Gd	Tb	Dy	Ho	Er	Tm	Yb	Lu	Hf
JL-U-01	14.4	69.1	3.93	16.7	6.05	2.02	17.8	5.62	64.7	25.2	123	27.6	269	57.4	11,975
JL-U-02	4.49	43.6	2.15	11.3	5.94	1.92	14.2	4.13	44.9	16.3	74.6	16.2	159	35.1	11,808
JL-U-03	113	296	29.2	117	19.8	4.28	23.8	6.17	65.7	24.0	113	24.8	251	55.4	10,905
JL-U-04	0.14	36.0	0.26	3.04	3.76	1.18	14.1	4.64	52.0	19.5	93.2	20.3	201	43.7	12,041
JL-U-05	54.2	156	16.6	73.8	12.8	1.82	15.8	3.66	42.0	15.8	74.9	17.6	182	41.0	12,484
JL-U-06	16.0	63.7	5.14	23.6	5.41	1.31	14.0	4.11	47.6	17.5	83.7	18.8	188	42.1	11,647
JL-U-07	5.48	42.2	1.99	9.89	4.10	0.72	11.9	3.50	43.5	17.0	84.4	18.7	192	43.8	11,190
JL-U-08	26.1	88.4	7.05	29.0	6.72	1.51	12.3	3.77	42.7	16.8	81.0	18.6	189	41.9	11,752
JL-U-09	7.3	26.6	0.042	0.97	2.05	0.60	9.93	3.25	39.5	16.1	78.9	18.3	189	43.4	12,680
JL-U-10	1.79	54.3	2.52	16.6	11.5	3.81	25.3	6.83	73.2	25.4	113	24.5	233	50.1	10,947
JL-U-11	31.8	113	10.3	45.7	9.2	1.55	17.2	4.77	58.1	24.2	126	29.8	313	71.2	12,653
JL-U-12	2.14	32.9	0.85	4.54	2.77	0.61	11.1	3.64	47.0	19.4	98	23.2	243	56.0	12,367
JL-U-13	22.7	82.2	6.88	29.6	6.70	1.36	13.0	3.75	41.5	16.1	78.7	18.2	186	41.8	12,362
JL-U-14	2.84	36.6	1.03	5.79	3.13	0.89	11.4	3.91	48.0	20.1	98.8	22.9	240	54.4	12,462
JL-U-15	16.6	73.5	5.98	28.6	6.43	1.39	13.6	4.14	47.3	18.9	90.3	21.1	216	49.8	11,889
JL-U-16	23.3	91.3	9.15	44.7	9.49	1.51	16.3	4.37	46.4	17.5	84.3	19.1	191	43.1	12,040
JL-U-17	7.15	56.7	3.10	15.8	6.88	2.70	19.0	5.70	61.0	21.3	96.2	20.8	203	43.5	10,285

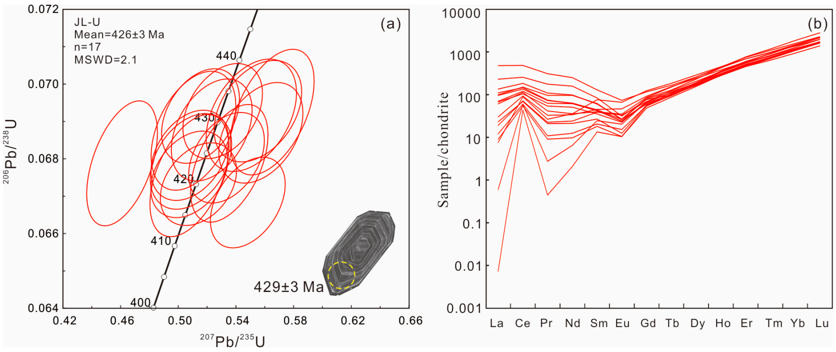

Figure 3. Cathodoluminescence (CL) and U-Pb concordia diagrams (**a**) and chondrite normalized REE pattern (**b**) of zircon crystals from the Jilongjie pluton.

Seventeen zircon grains had consistent or near-uniform $^{206}Pb/^{238}U$ ages ranging from 417 ± 3 Ma to 432 ± 3 Ma, with a weighted mean age of 426 ± 3 Ma (MSWD = 2.1, n = 17) (Figure 3a). The average age of Jilongjie plutonic rocks represents the crystallization age of the magmatic rocks, indicating that they were emplaced in the early Paleozoic.

4.2. Whole-Rock Geochemistry

Eleven representative samples were selected for whole-rock major element and trace element analyses (Table 3). Their loss on ignition (L.O.I.) range (1.83–3.04) suggests that Jilongjie plutonic rocks were insignificantly affected by alteration. Hence, we normalized the major element contents to 100% on a volatile-free basis. Jilongjie plutonic rocks had an SiO_2 content of 64.27–66.34 wt.%, K_2O content of 4.38–4.94 wt.%, Na_2O content of 2.50–2.93 wt.%, Al_2O_3 content of 12.95–14.31 wt.%, and total alkali ($K_2O + Na_2O$) content of 7.43–8.20. According to the total alkali–silica (TAS) diagram of igneous rocks proposed by Le Maitre [68], all Jilongjie plutons fall into the granite area (Figure 4a). In the $K_2O - SiO_2$ diagram, all samples fall into the shoshonite field [69]. The samples' A/CNK ($Al_2O_3/(CaO + Na_2O + K_2O)$) range was 0.80–1.04, and their A/NK ($Al_2O_3/(Na_2O + K_2O)$) range was 1.28–1.53. Therefore, in the A/CNK − A/NK diagram, Jilongjie granites fall into the meta-aluminous to weakly peraluminous fields [70]. In conclusion, Jilongjie pluton is shoshonitic granite.

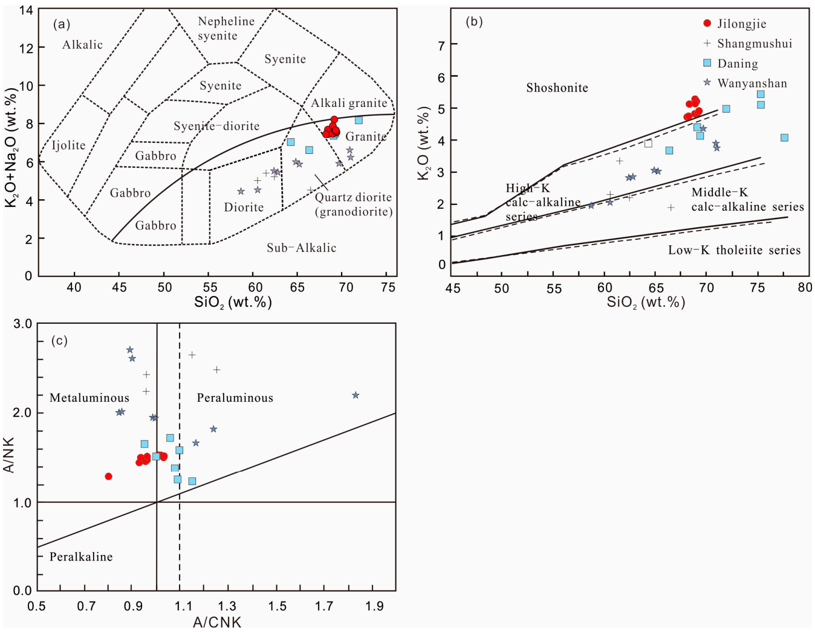

Figure 4. Geochemical characteristics of the Jilongjie pluton. (**a**) $SiO_2 - (Na_2O + K_2O)$ diagram [68]; (**b**) SiO_2–K_2O diagram [69]; (**c**) A/CNK–A/NK diagram [70]. Data sources: Nanmushui [45]; Daning [47]; and Wanyangshan [46].

Jilongjie granite contains 155.1–239.7 ppm of rare earth elements (∑REE). The chondrite-normalized rare earth element pattern suggests that Jilongjie granite has obvious enrichment of light rare earth elements relative to heavy rare earth elements ($(La/Yb)_N$ = 15.1–23.7) (Figure 5a). The samples showed a weak negative Eu anomaly, with Eu/Eu* in the 0.68–0.78 range (Figure 5a, Table 4). In the primitive-mantle-normalized trace element diagram, the samples clearly showed enrichment of large ion lithophile elements (such as Sr, Rb, and Ba) and depletion of high-field-strength elements (such as Nb, Ta, and Ti) (Figure 5b).

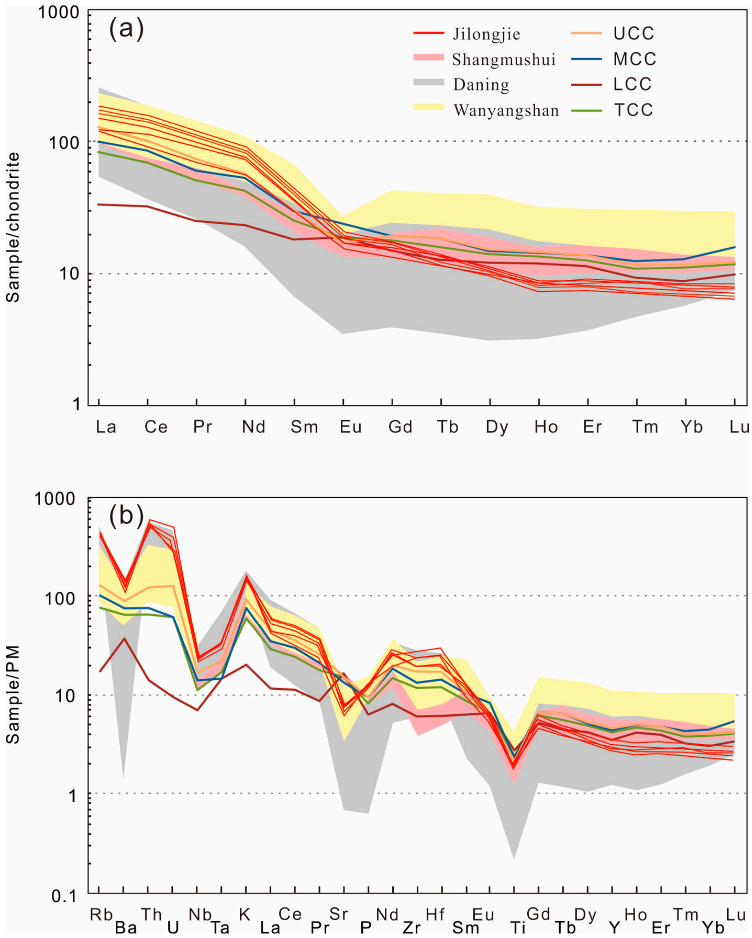

Figure 5. (**a**) Chondrite-normalized REE patterns; (**b**) Primitive-mantle-normalized trace element patterns. UCC—upper continental crust; MCC—middle continental crust; LCC—lower continental crust; TCC—total continental crust [71].

4.3. Zircon Hf Isotopic Results

Hafnium isotopic results and related parameters of 17 zircon grains of the Jilongjie granite samples are listed in Table 5. $^{176}Lu/^{177}Hf$ values were 0.001295–0.002283, $^{176}Yb/^{177}Hf$ values were 0.30414–0.56216, and $^{176}Hf/^{177}Hf$ values were 0.282502–0.282238 (Table 5). The Hf isotopic composition showed a wide variation; εHf(t) values were −9.94 to −0.69; model age values T_{DM} were 1.08–1.46 Ga, and two-stage model age values T_{DM2} were 1.46–2.04 Ga (Table 5).

Table 4. Major (wt.%) and trace element (ppm) concentrations of the Jilongjie granite.

Sample	JL-1H	JL-2H	JL-3H	JL-4H	JL-5H	JL-6H	JL-7H	JL-8H	JL-9H	JL-10H	JL-11H
Rock type						Granite					
SiO_2	65.48	64.95	64.70	66.34	64.27	65.47	65.81	65.22	65.22	65.97	65.70
TiO_2	0.53	0.55	0.52	0.55	0.55	0.57	0.57	0.56	0.54	0.52	0.52
Al_2O_3	14.31	13.79	14.18	13.94	13.61	12.95	14.07	13.83	14.01	13.87	13.72
$Fe_2O_3^T$	3.14	3.42	3.46	3.23	3.31	3.06	3.30	2.72	3.16	2.89	2.88
MnO	0.04	0.05	0.05	0.05	0.06	0.05	0.05	0.06	0.05	0.05	0.05
MgO	1.67	2.40	1.86	2.06	2.50	1.56	2.09	1.89	2.02	2.05	2.03
CaO	2.41	2.84	2.62	2.33	3.00	3.33	2.51	2.90	2.31	2.74	2.72
Na_2O	2.50	2.65	2.51	2.60	2.64	2.93	2.61	2.67	2.63	2.72	2.72
K_2O	4.94	4.44	4.77	4.62	4.38	4.87	4.54	4.79	4.62	4.56	4.55
P_2O_5	0.20	0.20	0.19	0.20	0.20	0.21	0.21	0.20	0.20	0.19	0.19
L.O.I	2.17	2.74	2.49	1.83	2.04	3.04	1.99	2.68	1.87	2.46	2.38
Total	99.38	100.01	99.34	99.73	99.57	100.03	99.73	99.52	99.63	100.01	99.46
A/CNK	1.03	0.96	1.01	1.03	0.94	0.80	1.02	0.93	1.04	0.96	0.96
A/NK	1.51	1.51	1.53	1.50	1.50	1.28	1.53	1.44	1.50	1.47	1.46
Mg#	51.26	58.13	51.51	55.79	59.92	50.22	55.57	57.85	55.93	58.41	58.24
					Trace element (ppm)						
Sc	10.8	10.0	11.0	10.9	10.9	8.49	11.0	11.0	10.9	9.49	9.31
V	67.0	69.0	67.3	69.8	72.4	56.2	70.5	70.6	69.8	64.1	63.3
Cr	150	153	149	160	161	156	150	159	158	143	142
Co	10.8	11.4	12.8	10.5	11.9	6.87	10.4	7.82	9.89	9.23	8.93
Ni	66.3	66.1	69.9	61.2	65.3	37.9	62.1	46.2	60.5	53.1	52.0
Ga	16.5	16.9	16.7	16.6	16.7	15.4	16.4	16.1	16.7	16.1	15.6
Rb	287	249	266	252	243	271	249	264	255	247	246
Sr	144	154	139	155	144	126	161	154	165	155	155
Y	15.4	14.0	16.3	14.0	15.3	13.6	14.2	14.5	13.2	13.0	12.8
Zr	287	211	211	284	310	265	274	308	267	226	217
Nb	17.1	16.7	15.8	16.7	17.1	16.5	16.8	16.8	16.5	15.4	15.2
Ba	787	990	742	942	1012	918	836	935	885	923	931
La	41.8	41.9	37.9	40.2	36.6	28.6	44.1	29.5	41.1	38.8	35.8
Ce	88.9	89.3	81.8	88.0	81.9	56.8	97.6	70.3	89.4	87.6	79.1
Pr	10.0	10.4	9.53	10.4	9.73	6.61	11.4	8.72	10.4	10.1	9.30
Nd	38.5	39.7	36.4	39.2	37.2	26.4	42.9	34.6	39.6	38.3	35.7
Sm	5.78	5.97	5.93	6.02	5.87	4.39	6.55	5.80	5.97	5.79	5.28

Table 4. *Cont.*

Sample	JL-1H	JL-2H	JL-3H	JL-4H	JL-5H	JL-6H	JL-7H	JL-8H	JL-9H	JL-10H	JL-11H
Eu	1.05	1.07	1.11	1.09	1.13	0.90	1.19	0.99	1.11	1.06	1.00
Gd	3.54	3.64	3.83	3.59	3.72	2.80	3.50	3.39	3.43	3.42	3.13
Tb	0.51	0.49	0.53	0.49	0.50	0.43	0.51	0.50	0.48	0.45	0.44
Dy	2.91	2.76	3.05	2.74	2.97	2.57	2.83	2.83	2.57	2.58	2.44
Ho	0.51	0.48	0.54	0.48	0.51	0.45	0.48	0.50	0.46	0.45	0.41
Er	1.52	1.35	1.62	1.40	1.52	1.30	1.50	1.44	1.39	1.31	1.24
Tm	0.22	0.20	0.24	0.22	0.22	0.20	0.22	0.22	0.22	0.18	0.18
Yb	1.53	1.27	1.54	1.37	1.45	1.29	1.41	1.40	1.30	1.18	1.13
Lu	0.21	0.17	0.22	0.20	0.21	0.18	0.21	0.20	0.19	0.17	0.16
Hf	8.04	6.12	6.06	8.21	8.79	7.81	8.04	9.15	7.98	6.49	6.37
Ta	1.40	1.32	1.43	1.33	1.35	1.38	1.36	1.38	1.35	1.24	1.19
Pb	34.1	35.5	35.4	37.9	33.6	39.2	39.4	40.1	38.8	36.4	37.3
Th	45.0	49.8	44.6	50.3	44.9	51.5	47.8	47.3	44.9	52.0	48.1
U	6.47	5.34	7.63	6.41	5.56	10.4	6.23	7.05	8.33	6.20	5.76
∑REE	223.16	222.64	211.59	220.30	209.81	155.07	239.67	185.96	221.71	213.82	197.45
$(La/Yb)_N$	19.58	23.72	17.69	21.04	18.16	15.87	22.40	15.12	22.62	23.58	22.82
Eu/Eu*	0.71	0.71	0.71	0.72	0.74	0.78	0.76	0.68	0.75	0.73	0.75

Eu/Eu* = $\frac{Eu_N}{\sqrt{(Sm_N)\times(Gd_N)}}$.

Table 5. Zircon Hf isotopic in situ analysis results and related parameters.

Sample No.	Age/Ma	$^{176}Yb/^{177}Hf$	2σ	$^{176}Lu/^{177}Hf$	2σ	$^{176}Hf/^{177}Hf$	2σ	εHf(0)	εHf(t)	T_{DM}(Ga)	$T_{DM}{}^{C}$ (Ga)	$f_{Lu/Hf}$
JL-U-01	423	0.0356	0.0010	0.001495	0.000038	0.282353	0.000024	−14.82	−5.94	1.29	1.78	−0.95
JL-U-02	431	0.0534	0.0006	0.002153	0.000027	0.282502	0.000014	−9.56	−0.69	1.09	1.46	−0.94
JL-U-03	421	0.0353	0.0003	0.001411	0.000021	0.282422	0.000019	−12.37	−3.50	1.19	1.63	−0.96
JL-U-04	432	0.0562	0.0006	0.002283	0.000024	0.282378	0.000013	−13.93	−5.08	1.28	1.74	−0.93
JL-U-05	428	0.0314	0.0005	0.001303	0.000021	0.282305	0.000014	−16.52	−7.48	1.35	1.89	−0.96
JL-U-06	424	0.0417	0.0006	0.001740	0.000021	0.282424	0.000015	−12.30	−3.46	1.19	1.63	−0.95
JL-U-07	423	0.0374	0.0006	0.001508	0.000026	0.282260	0.000015	−18.10	−9.22	1.42	1.99	−0.95
JL-U-08	429	0.0482	0.0007	0.001979	0.000024	0.282324	0.000018	−15.84	−6.96	1.34	1.85	−0.94
JL-U-09	425	0.0332	0.0006	0.001387	0.000025	0.282336	0.000022	−15.43	−6.48	1.31	1.82	−0.96
JL-U-10	429	0.0337	0.0022	0.001377	0.000088	0.282347	0.000015	−15.03	−5.98	1.29	1.79	−0.96
JL-U-11	420	0.0423	0.0007	0.001754	0.000023	0.282501	0.000017	−9.57	−0.81	1.08	1.46	−0.95
JL-U-12	422	0.0394	0.0015	0.001636	0.000059	0.282366	0.000017	−14.37	−5.55	1.27	1.76	−0.95
JL-U-13	417	0.0362	0.0010	0.001481	0.000038	0.282323	0.000014	−15.88	−7.12	1.33	1.85	−0.96
JL-U-14	432	0.0373	0.0011	0.001540	0.000041	0.282430	0.000015	−12.09	−3.03	1.18	1.61	−0.95
JL-U-15	424	0.0530	0.0021	0.002127	0.000089	0.282398	0.000016	−13.23	−4.50	1.24	1.69	−0.94
JL-U-16	431	0.0462	0.0006	0.001863	0.000022	0.282238	0.000034	−18.88	−9.94	1.46	2.04	−0.94
JL-U-17	432	0.0304	0.0007	0.001295	0.000029	0.282264	0.000016	−17.98	−8.85	1.41	1.98	−0.96

5. Discussion

5.1. Genetic Type and Magma Source

Granite's genesis and geodynamic mechanisms are closely related to rock types [72]. Whalen, et al. [73] proposed that A, I, S, and M-type granites can be distinguished according to rocks' geochemical characteristics, such as FeO*/MgO and the Y vs. 10,000 × Ga/Al discriminant diagram. In the discrimination diagram, all samples fall into I, S, and M regions, indicating that they are not A-type granites (Figure 6a,b). I-type granites are generally calcium-rich and aluminum-poor, with a high Na_2O/K_2O ratio, and are mostly meta-aluminous (A/CNK < 1.1). I-type granites' dark minerals mostly contain clinopyroxene or amphibole. S-type granites are rich in aluminum but low in calcium, with a low Na_2O/K_2O ratio. They are peraluminous (A/CNK > 1.1), and contain metamorphic minerals such as sillimanite, cordierite, garnet, and andalusite [74]. Jilongjie plutonic rocks are meta-aluminous to weakly peraluminous (A/CNK = 0.80–1.04) and contain amphiboles (Figure 2), which are similar to I-type granites. Moreover, the Jilongjie pluton falls into the I-type granite region in the Rb/Zr vs. SiO_2 plot (Figure 6c), as well as the I-type granite trend in the P_2O_5 vs. SiO_2 plot (Figure 6d). Therefore, its petrological and petrochemical characteristics indicate that Jilongjie granite is an I-type granite.

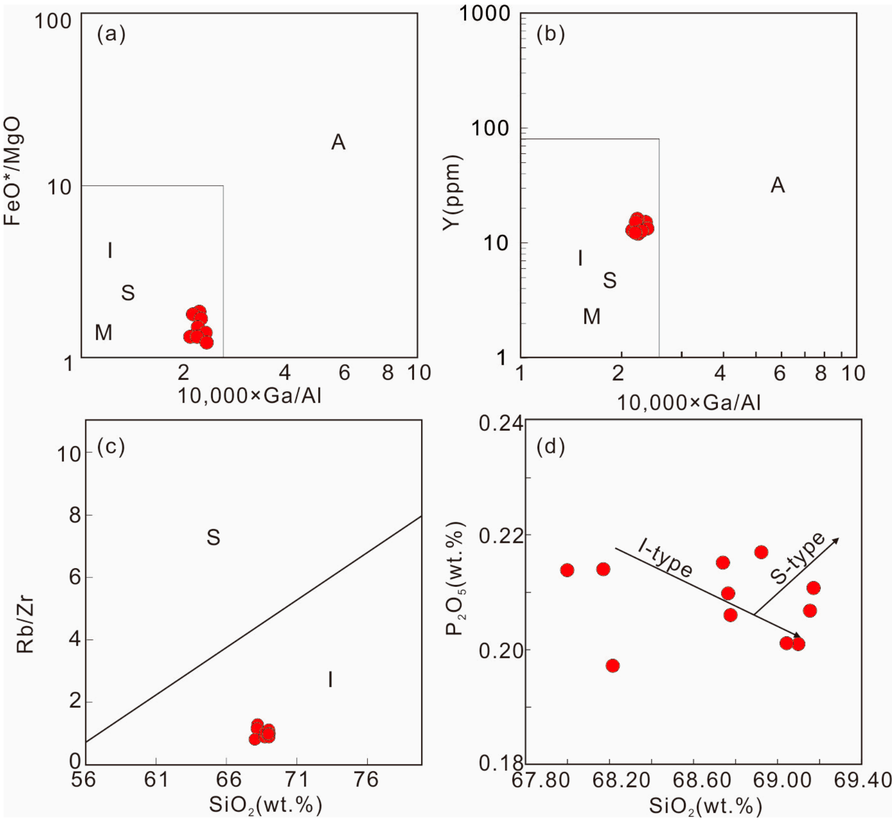

Figure 6. Chemical discrimination diagrams for I-, S-, M, and A-type granites; (**a**) 10,000× Ga/Al vs. FeO*/MgO [75]; (**b**) 10,000× Ga/Al vs. Y [75]; (**c**) Rb/Zr vs. SiO_2 [76]; and (**d**) P_2O_5 vs. SiO_2 [77].

5.2. Magma Source

Generally, the following models could account for the generation of I-type granite: (1) partial melting of metamorphic intermediate-mafic volcanic rocks [78–80]; (2) fractionation from the mantle-derived mafic magma [81,82]; (3) partial melting of juvenile crust induced by asthenosphere underplating [83,84]; and (4) mixing between mantle-derived mafic- and crust-derived felsic magma [85–88].

I-type granites generated by the fractional crystallization of mantle–derived mafic magma ordinarily have the following characteristics [81,82,89]: (1) massive ultramafic and mafic lavas exposed around the study area; (2) samples with obvious negative Eu and Sr anomalies, indicating that magma formation was the result of the fractional crystallization of plagioclase from ultramafic and mafic melts; (3) the occurrence of mafic enclaves; and (4) enrichment with Sr-Nd-Pb isotopic features. The geological and geochemical characteristics of the Jilongjie pluton rule out fractional crystallization of mantle-derived mafic magma.

Zircon grains from Jilongjie granite samples had negative ε_{Hf}(t) values ranging from −9.9 to −0.7 (Figure 7); this rules out partial melting of metamorphic intermediate-mafic volcanic rocks and fractionation from mantle-derived mafic magma (Figure 7). Based on these negative ε_{Hf}(t) values and the model age of 1.04–1.46 Ga, the most direct explanation is that they originated from the anatexis or remelting of ancient crustal materials [90]. However, zircon Hf isotope data show obvious inhomogeneity (its variation range was several ε units); this required an open system to cause remarkable changes in the ^{176}Hf/^{177}Hf ratio in the melt (Figure 7) [91]. As zircon Hf isotope ratios hardly change with partial melting or fractional crystallization, the heterogeneity of zircon Hf isotopes likely indicates the interaction of mantle- and crust-derived magmas [92]. Therefore, similar to the heterogeneity of zircon Hf isotopes observed in other parts of the world, the Jilongjie pluton with similar characteristics is also interpreted as the result of the mixing of mantle- and crust-derived magmas [77,91–94]. Previous studies indicated that igneous rock with a high transition metal content are generally interpreted as direct melting from mantle peridotite or mixed melting from crust and mantle materials [95,96]. The high content of transition metals in Jilongjie granite was most likely derived from the mixed melting of crustal and mantle materials (Table 4). Moreover, in the (La/Yb)$_N$ diagram, the Jilongjie pluton falls into a mixed mantle and crust region (Figure 7c).

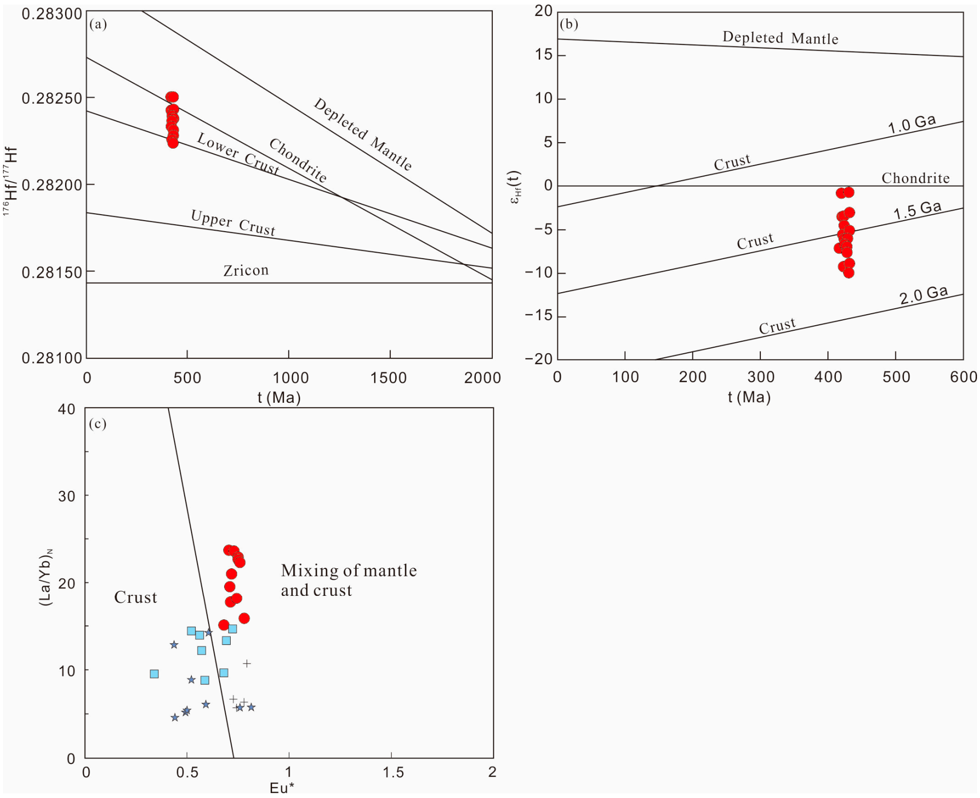

Figure 7. (**a**) (^{176}Hf/^{177}Hf) vs. t (Ma); (**b**) ε_{Hf} (t) vs. t (Ma) [97]; (**c**) (La/Yb)$_N$ vs. Eu/Eu* [98]. The data source is the same as that in Figure 4. The legends are the same as Figure 4.

However, it is difficult to explain the whole-rock major and trace geochemical characteristics of Jilongjie pluton based solely on the mixing of mantle- and crust-derived material.

The depletion of Ba, Nb, Ta, Sr, and Ti indicate that its parent magma has undergone significant fractional crystallization (Figure 5). For example, the depletion of Nb, Ta, and Ti indicates the fractional crystallization of titanium-rich mineral phases (such as ilmenite and/or rutile) and Ca-amphibole, and the strong depletion of Sr and Ba indicates the fractional crystallization of plagioclase and potassium feldspar. Moreover, the Rb vs. Sr and Ba vs. Sr diagrams also suggest fractional crystallization of plagioclase and potassium feldspar (Figure 8a,b). Fractional crystallization of zircon and K-feldspar are also indicated in Zr vs. SiO_2 and Ba vs. SiO_2 diagrams, respectively (Figure 8c,d).

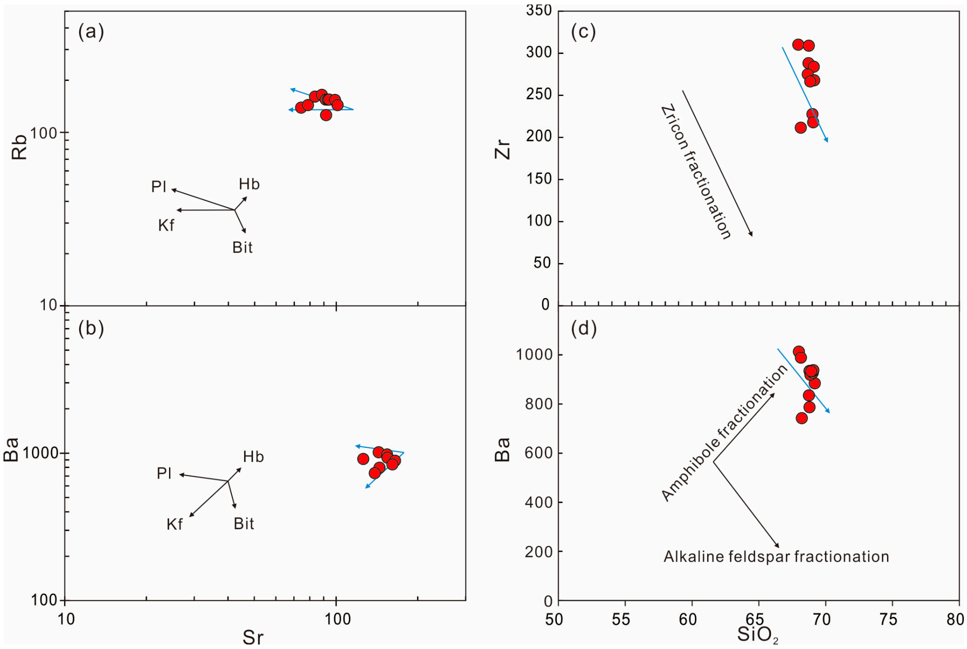

Figure 8. (**a**) Rb vs. Sr; (**b**) Ba vs. Sr; (**c**) Zr vs. SiO_2; and (**d**) Ba vs. SiO_2 diagrams of granite in the Jilongjie area (after Zong, et al. [99]). Mineral abbreviations are the same as Figure 2.

Mantle material may have played an important role in the SCB's Triassic magmatism, including the Shangmushui, Daning, and Wanyangshan plutons [45–47]. The geochemical characteristics of Jilongjie granite are similar to those of the above plutons (Figures 4 and 5). Therefore, based on geological, major and trace element geochemical, and Hf isotope data, we suggest that the parent magma of Jilongjie granite originated from mixed crust-derived felsic and mantle-derived mafic magmas, followed by fractional crystallization during its ascent or in the emplacement level.

5.3. Tectonic Implications

According to previous studies, granites and granitic gneisses dated from the Late Ordovician to the Early Devonian are considered the significant products of early Paleozoic magmatism in the SCB [37–39,44,100–102]. The early Paleozoic Wuyi–Yunkai orogeny in the SCB was the first extensive tectonothermal event since the Neoproterozoic break-up of the Rodinia supercontinent, roughly synchronized with the Caledonian orogeny in Europe [1,103,104]. However, the tectonic–magmatic evolution of the early Paleozoic remains controversial. Some scholars suggest that the Wuyi–Yunkai orogeny was the result of continental collisions or arc collisions caused by the subduction and closure of the Huanan Ocean between the Cathaysian and Yangtze blocks during the Caledonian period [105–107]. Others argue that the Yangtze and Cathaysian blocks were still continuous in the early Paleozoic, and thus the Wuyi–Yukai orogeny represents an intracontinental collision [7,14,37,108–110]. The following petrological and sedimentary geological features indicate that the Wuyi–Yunkai orogeny was more likely an intraplate orogeny rather than a subduction-related orogenic event: (1) Using statistics from previous research, we found that massive granites are widely distributed, which is inconsistent with the linear distribution of magmatic rocks in the subduction mode (Figure 1a; [6]). (2) Early Paleozoic ophiolitic suites, arc andesites, and calc-alkaline volcanic rocks related to the closure of the Huanan Ocean (mentioned above) are absent [12,14,109]. (3) The paleoecological and biostratigraphical evolution in the Cathaysia and Yangtze blocks are related and continuous [111]. (4) The age spectra of detrital zircon from lower Paleozoic sandstones of the Cathaysia and Yangtze blocks have similar characteristics [109,112].

Although the Jilongjie pluton is a significant distance from the Wuyi–Yunkai orogeny's core area, according to its temporal and spatial distribution characteristics, it is likely to be the westward extension of the orogenic belt or the product of early Paleozoic granitic magmatism [31,113]. Therefore, it should have been generated in the same tectonic setting. However, it is controversial whether the tectonic setting of the early Paleozoic magmatic rocks (especially 460–400 Ma) in the South China Plate was syn-collisional [43,113] or post-collisional [26,27,37,39,44,100,101]. As shown in Figure 9, Jilongjie granites plot in the field of syn-collisional to post-collisional granites.

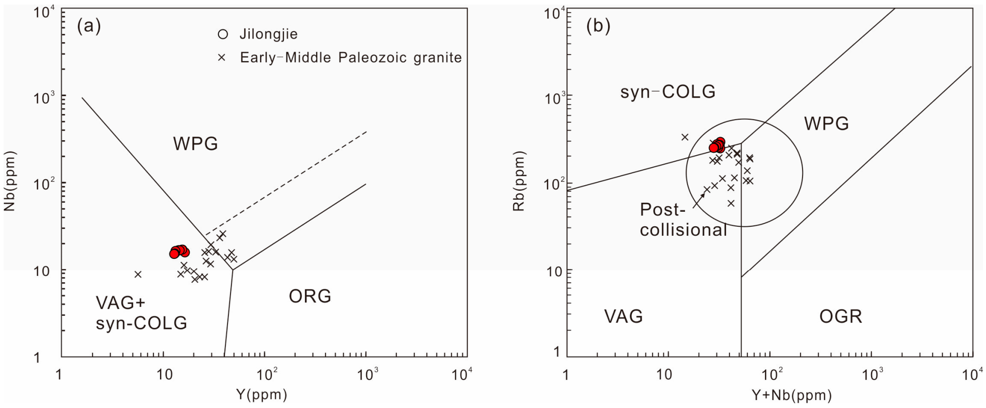

Figure 9. (**a**) Y vs. Nb and (**b**) (Y + Nb) vs. Rb [114]. The data source is the same as Figure 4.

Increasing evidence indicates that extensional mechanisms related to the post-collision stage were responsible for the generation of magmatic rocks in the SCB after 435 Ma, as follows: (1) Massive granites are widely distributed in the SCB, which is inconsistent with the characteristics of a small amount of migmatite and leucogranite generated in the syn-collisional orogenic stage [115]. (2) The high-magnesium basalt in the Wuyi–Yunkai orogenic belt indicates that the potential temperature of mantle melting at that time exceeded 1300 °C, which is significantly different from the syn-collision extrusion regime [42]. (3) The mafic intrusive rocks and contemporaneous granitic rocks generated by the decompression melting of the mantle in the SBC due to lithospheric extension are characterized by a bimodal pattern, which is consistent with post-collision extensional magmatism rather than a compression regime [26,101]. (4) Recent studies of deformation and advanced metamorphism indicate a prograde metamorphism associated with synorogenic crustal thickening and a retrograde metamorphism with postorogenic rapid exhumation at 460–435 and 435–400 Ma, respectively [26,27,100].

In summary, we suggest that the tectonic–magmatic evolution model of the Early Paleozoic (460–400 Ma) in the SCB can be summarized as follows: (1) During the syn-collision period (460–435 Ma), the crust was significantly shortened and thickened, causing high-temperature crustal anatexis and generating granitic rocks, accompanied by thickening of the lithospheric root (Figure 10a) [7,26,37,39]; (2) between 435 and 400 Ma, as the lithosphere was denser than the underlying asthenosphere, delamination caused part of the lithosphere root to be removed [116]. The subsequent upwelling of the asthenosphere provided heat to melt the lithospheric mantle [117]. The partial melting of the depleted lithosphere produced mafic magma, which intruded into the middle and upper crust, forming a huge magma chamber [118]. The intrusive mafic magma promoted massive crustal melting and generated granitic melts [117]. Subsequently, the depleted mantle-derived material mixed with the granitic parent magma, generating intermediate granites, including the Jilongjie pluton (Figure 10b).

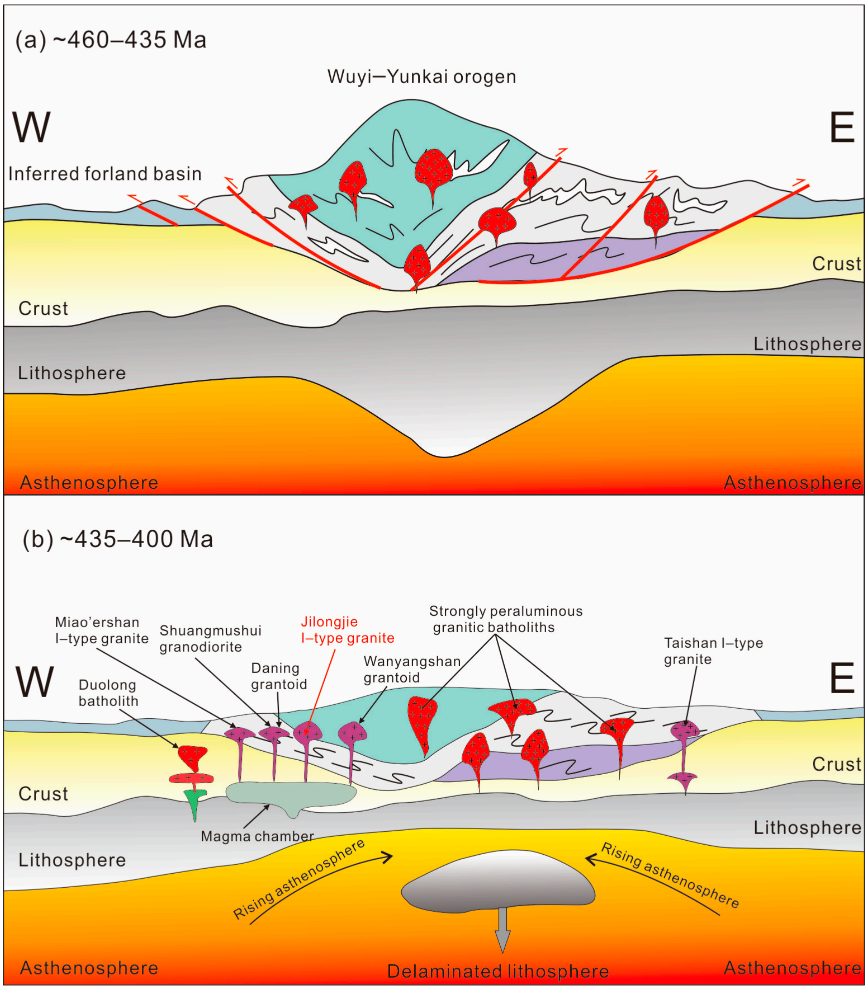

Figure 10. Simplified diagrams showing (**a**) ~460–135 Ma, crustal thickening and (**b**) ~435–400 Ma, lithospheric delamination in central SCB (modified after [101]). Data sources: Duolong batholith [44]; Miao'ershan I-type granite [27]; Taishan I-type granite [41]; strongly peraluminous granitic batholiths [37,39,119].

6. Conclusions

(1) The Jilongjie pluton was emplaced at ~426 Ma and displays shoshonite and metaluminous characteristics.
(2) Jilongjie granites' parent magma originated from a mixing of crust-derived felsic and mantle-derived mafic magmas, and then underwent fractional crystallization during its ascent and/or emplacement.
(3) The post-collisional extensional mechanism associated with the delamination of the thickened lithosphere was responsible for post-435 Ma igneous rock (including the Jilongjie pluton) in the SCB.

Author Contributions: Conceptualization, T.W.; Data curation, Q.S. and X.D.; Formal analysis, X.R., D.H. and Y.X.; Funding acquisition, H.Z. and L.C.; Investigation, S.L. and P.F.; Methodology, Q.S.; Resources, Q.S.; Software, Y.X.; Writing—original draft, H.H.; Writing—review and editing, H.H. and L.C. All authors have read and agreed to the published version of the manuscript.

Funding: The research was financially supported by the Natural Science Foundation of Hunan Province, China (Grant No. 2023JJ30507, 2023JJ30505 and 2023JJ30508); the Research Foundation of the Education Bureau of Hunan Province, China (Grant No. 22B0433 and 22A0294); and the Open Research Fund from the State Key Laboratory of Nuclear Resources and Environment (East China University of Technology) (2022NRE08).

Data Availability Statement: Not applicable.

Acknowledgments: We are grateful to the editor-in-chief and reviewers.

Conflicts of Interest: The authors declare no conflict of interest.

References

1. Li, X.H.; Li, Z.X.; Zhou, H.W.; Liu, Y.; Kinny, P.D. U–Pb zircon geochronology, geochemistry and Nd isotopic study of Neoproterozoic bimodal volcanic rocks in the Kangdian Rift of South China: Implications for the initial rifting of Rodinia. *Precambrian Res.* **2002**, *113*, 135–154. [CrossRef]
2. Li, Z.X.; Li, X.H.; Li, W.X.; Ding, S.J. Was Cathaysia part of Proterozoic Laurentia?–New data from Hainan Island, south China. *Terra. Nova* **2008**, *20*, 154–164. [CrossRef]
3. Li, Z.X.; Zhang, L.H.; Powell, C.M. South China in Rodinia: Part of the missing link between Australia–East Antarctica and Laurentia? *Geology* **2015**, *23*, 407–410. [CrossRef]
4. Zhou, X.M.; Zhu, Y.H. Late Proterozoic colisional orogen and geosuture in Southeastern China- Petrological evidence. *Chin. J. Geochem.* **1993**, *12*, 239–251.
5. Charvet, J.; Shu, L.; Shi, Y.S.; Guo, L.Z.; Faure, M. The building of south China: Collision of Yangzi and Cathaysia blocks, problems and tentative answers. *J. Southeast Asian Earth Sci.* **1996**, *13*, 223–235. [CrossRef]
6. Sun, T. A new map showing the distribution of granites in South China and its explanatory notes. *Geol. Bull. China* **2006**, *25*, 332–335.
7. Wang, Y.; Fan, W.; Zhao, G.; Ji, S.; Peng, T. Zircon U–Pb geochronology of gneissic rocks in the Yunkai massif and its implications on the Caledonian event in the South China Block. *Gondwana Res.* **2007**, *12*, 404–416. [CrossRef]
8. Ren, J.S. On the Geotectonics of Southern China. *Acta Geol. Sin.* **1991**, *4*, 111–130.
9. Li, Z.X.; Li, X.H. Formation of the 1300-km-wide intracontinental orogen and postorogenic magmatic province in Mesozoic South China: A flat-slab subduction model. *Geology* **2007**, *35*, 179. [CrossRef]
10. Shu, L.S. Predevonian Tectonic Evolution of South China:from Cathaysian Block to Caledonian Period FoldedOrogenic Belt. *Geol. J. China Univ.* **2006**, *12*, 418–431.
11. Chen, X.; Zhang, Y.; Fan, J.; Cheng, J.; Li, Q. Ordovician graptolite-bearing strata in southern Jiangxi with a special reference to the Kwangsian Orogeny. *Sci. China Earth Sci.* **2011**, *53*, 1602–1610. [CrossRef]
12. Shu, L.; Faure, M.; Wang, B.; Zhou, X.; Song, B. Late Palaeozoic–Early Mesozoic geological features of South China: Response to the Indosinian collision events in Southeast Asia. *Comptes Rendus Geosci.* **2008**, *340*, 151–165. [CrossRef]
13. Shu, L.S.; Deng, P.; Yu, J.H.; Wang, Y.B.; Jiang, S.Y. The age and tectonic environment of the rhyolitic rocks on the western side of Wuyi Mountain, South China. *Sci. China Ser. D Earth Sci.* **2008**, *51*, 1053–1063. [CrossRef]
14. Shu, L.S.; Yu, J.H.; Jia, D.; Wang, B.; Shen, W.Z.; Zhang, Y.Q. Early Paleozoic orogenic belt in the eastern segment of South China. *Geol. Bull. China* **2008**, *27*, 1581–1593.
15. Wang, Y.; Fan, W.; Guo, F.; Peng, T.; Li, C. Geochemistry of Mesozoic Mafic Rocks Adjacent to the Chenzhou-Linwu fault, South China: Implications for the Lithospheric Boundary between the Yangtze and Cathaysia Blocks. *Int. Geol. Rev.* **2003**, *45*, 263–286. [CrossRef]
16. Wang, Y.; Fan, W.; Sun, M.; Liang, X.; Zhang, Y.; Peng, T. Geochronological, geochemical and geothermal constraints on petrogenesis of the Indosinian peraluminous granites in the South China Block: A case study in the Hunan Province. *Lithos* **2007**, *96*, 475–502. [CrossRef]
17. Wang, Y.; Zhang, Y.; Fan, W.; Peng, T. Structural signatures and 40Ar/39Ar geochronology of the Indosinian Xuefengshan tectonic belt, South China Block. *J. Struct. Geol.* **2005**, *27*, 985–998. [CrossRef]
18. Wang, Y.J.; Zhang, Y.; Fang, W.M.; Xi, X.W.; Guo, F.; Li, G. Numerical modeling for generation of Indo–Sinian peraluminous granitoids Hunan Province: Basaltic underplating vs tectonic thickening. *Sci. China (Ser. D)* **2002**, *45*, 1042–1056. [CrossRef]
19. Bao, H.Z.; Zhang, Z.C. Genesis of Silicic Large Igneous Provinces and effects of resources and environment. *Acta Petrol. Sin.* **2020**, *36*, 1973–1985. [CrossRef]
20. Chen, A. Mirror-image thrusting in the South China Orogenic Belt: Tectonic evidence from western Fujian, southeastern China. *Tectonophysics* **1999**, *305*, 497–519. [CrossRef]
21. Mao, J.W.; Xie, Z.Q.; Guo, C.L.; Yuan, C.D.; Cheng, Y.B.; Chen, Y.C. Spatial-Temporal distribution of Mesozoic ore deposits in South China and their metallogenic settings. *Geol. J. China Univ.* **2008**, *14*, 510–526. [CrossRef]
22. Zhang, Q.; Jin, W.J.; Li, C.D.; Wang, Y.L. Yanshanian large-scale magmatism and lithosphere thinning in Eastern China: Relation to large igneous province. *Earth Sci. Front.* **2009**, *16*, 21–51.

23. Wan, Y.; Liu, D.; Xu, M.; Zhuang, J.; Song, B.; Shi, Y.; Du, L. SHRIMP U–Pb zircon geochronology and geochemistry of metavolcanic and metasedimentary rocks in Northwestern Fujian, Cathaysia block, China: Tectonic implications and the need to redefine lithostratigraphic units. *Gondwana Res.* **2007**, *12*, 166–183. [CrossRef]
24. Shen, W.Z.; Ling, H.F.; Li, W.X.; Wang, D.Z.; Huang, X.; Pan, J. The Nd-Sr isotope study of Mesozoic granitoids in Jiangxi Province. *Chin. Sci. Bull.* **1998**, *43*, 2653–2657. [CrossRef]
25. Chen, J.F.; Jahn, B.M. Crustal evolution of southeastern China: Nd and Sr isotopic evidence. *Tectonophysics* **1998**, *284*, 101–133. [CrossRef]
26. Li, Z.X.; Li, X.H.; Wartho, J.A.; Clark, C.; Li, W.X.; Zhang, C.L.; Bao, C. Magmatic and metamorphic events during the early Paleozoic Wuyi-Yunkai orogeny, southeastern South China: New age constraints and pressure-temperature conditions. *Geol. Soc. Am. Bull.* **2009**, *122*, 772–793. [CrossRef]
27. Zhao, K.-D.; Jiang, S.-Y.; Sun, T.; Chen, W.-F.; Ling, H.-F.; Chen, P.-R. Zircon U–Pb dating, trace element and Sr–Nd–Hf isotope geochemistry of Paleozoic granites in the Miao'ershan–Yuechengling batholith, South China: Implication for petrogenesis and tectonic–magmatic evolution. *J. Asian Earth Sci.* **2013**, *74*, 244–264. [CrossRef]
28. Li, X.; Tatsumoto, M.; Premo, W.R. Age and origin of the Tanghu Granite, south. *Geology* **1989**, *17*, 395–399.
29. Li, X.H. Geochronology of the Wanyangshan–Zhuguangshan granitoid batholith: Implication for the crust development. *Sci. China Ser. B* **1991**, *34*, 620–629.
30. Wang, J.H.; Sun, D.Z.; Chang, X.Y.; Deng, S.X.; Zhang, H.; Zhou, H.W. U–Pb dating of the Napeng granite at the NW margin of the Yunkai block, Guangdong, South China. *Acta Mineral. Sin.* **1998**, *18*, 130–133.
31. Roger, F.; Leloup, P.H.; Jolivet, M.; Lacassin, R.; Trinh, P.T.; Brunel, M.; Seward, D. Long and complex thermal history of the Song Chay metamorphic dome (Northern Vietnam) by multi-system geochronology. *Tectonophysics* **2000**, *321*, 449–466. [CrossRef]
32. Xu, X.; O'Reilly, S.Y.; Griffin, W.L.; Deng, P.; Pearson, N.J. Relict Proterozoic basement in the Nanling Mountains (SE China) and its tectonothermal overprinting. *Tectonics* **2005**, *24*, 1–16. [CrossRef]
33. Chen, C.H.; Lee, C.Y.; Hsieh, P.S.; Zeng, W.; Zhou, H.W. Approaching the age problem for some metamorphosed Precambrian basement rocks and Phanerozoic granitic bodies in the Wuyi area: The application of EMP monazite age dating. *Geol. J. China Univ.* **2008**, *14*, 1–15. [CrossRef]
34. Liu, R.; Zhang, L.; Zhou, H.W.; Zhong, Z.Q.; Zeng, W.; Xiang, H.; Ji, S.; Lv, X.Q.; Li, C.Z. Petrogenesis of the Caledonian migmatites and related granites in northwestern Fujian Province, South China: Syndeformational crustal anatexis. *Acta Petrol. Sin.* **2008**, *24*, 1205–1222.
35. Zeng, W.; Zhang, L.; Zhou, H.; Zhong, Z.; Xiang, H.; Liu, R.; Jin, S.; Lü, X.; Li, C. Caledonian reworking of Paleoproterozoic basement in the Cathaysia Block: Constraints from zircon U-Pb dating, Hf isotopes and trace elements. *Sci. Bull.* **2008**, *53*, 895–904. [CrossRef]
36. Wan, Y.; Liu, D.; Wilde, S.A.; Cao, J.; Chen, B.; Dong, C.; Song, B.; Du, L. Evolution of the Yunkai Terrane, South China: Evidence from SHRIMP zircon U–Pb dating, geochemistry and Nd isotope. *J. Asian Earth Sci.* **2010**, *37*, 140–153. [CrossRef]
37. Wang, Y.; Zhang, A.; Fan, W.; Zhao, G.; Zhang, G.; Zhang, Y.; Zhang, F.; Li, S. Kwangsian crustal anatexis within the eastern South China Block: Geochemical, zircon U–Pb geochronological and Hf isotopic fingerprints from the gneissoid granites of Wugong and Wuyi–Yunkai Domains. *Lithos* **2011**, *127*, 239–260. [CrossRef]
38. Zhang, A.; Wang, Y.J.; Fan, W.M.; Zhang, F.F.; Zhang, Y.Z. LA-ICPMS zircons U–Pb geochronology and Hf isotopic composition of the Taoxi migmatite (Wuping): Constrains on the formation age of the Taoxi complex and the Yu'nan event. *Geotecton. Et Metallog.* **2011**, *35*, 64–72.
39. Zhang, F.; Wang, Y.; Zhang, A.; Fan, W.; Zhang, Y.; Zi, J. Geochronological and geochemical constraints on the petrogenesis of Middle Paleozoic (Kwangsian) massive granites in the eastern South China Block. *Lithos* **2012**, *150*, 188–208. [CrossRef]
40. Chu, Y.; Lin, W.; Faure, M.; Wang, Q.; Ji, W. Phanerozoic tectonothermal events of the Xuefengshan Belt, central South China: Implications from UPb age and LuHf determinations of granites. *Lithos* **2012**, *150*, 243–255. [CrossRef]
41. Huang, X.-L.; Yu, Y.; Li, J.; Tong, L.-X.; Chen, L.-L. Geochronology and petrogenesis of the early Paleozoic I-type granite in the Taishan area, South China: Middle-lower crustal melting during orogenic collapse. *Lithos* **2013**, *177*, 268–284. [CrossRef]
42. Yao, W.-H.; Li, Z.-X.; Li, W.-X.; Wang, X.-C.; Li, X.-H.; Yang, J.-H. Post-kinematic lithospheric delamination of the Wuyi–Yunkai orogen in South China: Evidence from ca. 435Ma high-Mg basalts. *Lithos* **2012**, *154*, 115–129. [CrossRef]
43. Wang, D.; Zheng, J.; Ma, Q.; Griffin, W.L.; Zhao, H.; Wong, J. Early Paleozoic crustal anatexis in the intraplate Wuyi–Yunkai orogen, South China. *Lithos* **2013**, *175–176*, 124–145. [CrossRef]
44. Peng, T.; Fan, W.; Zhao, G.; Peng, B.; Xia, X.; Mao, Y. Petrogenesis of the early Paleozoic strongly peraluminous granites in the Western South China Block and its tectonic implications. *J. Asian Earth Sci.* **2015**, *98*, 399–420. [CrossRef]
45. Zou, Y.; Nong, N.J.; Guo, S.Y.; Huang, X.Q.; Sun, M.X. Petrogenesis of the shangmushui pluton in southeast Guangxi province: Constraints from petrochemistry, zircon U-Pb ages and Hf isotope. *J. Mineral. Petrol.* **2017**, *37*, 52–62. [CrossRef]
46. Chen, D.; Ma, T.Q.; Liu, W.; Liu, Y.R.; Ma, A.J.; Ni, Y.J. Zircon SHRIMP U-Pb Age, Petrogenesis and Tectonic Implication of Wanyangshan Pluton in Southeast Hunan Province. *Geotecton. Et Metallog.* **2016**, *40*, 873–890. [CrossRef]
47. Cheng, S.B.; Fu, J.M.; Xu, D.M.; Chen, X.Q.; Ma, L.Y.; Wang, X.D.; Pang, Y.C. Zircon SHRIMP U-Pb dating and geochemical characteristics of Daning batholith in northeast Guangxi. *Geol. China* **2009**, *36*, 1278–1288. [CrossRef]
48. Wang, Y.; Fan, W.; Cawood, P.A.; Li, S. Sr–Nd–Pb isotopic constraints on multiple mantle domains for Mesozoic mafic rocks beneath the South China Block hinterland. *Lithos* **2008**, *106*, 297–308. [CrossRef]

49. Liu, X.; Gao, S.; Diwu, C.; Ling, W. Precambrian crustal growth of Yangtze Craton as revealed by detrital zircon studies. *Am. J. Sci.* **2008**, *308*, 421–468. [CrossRef]
50. Shu, L.; Faure, M.; Jiang, S.; Yang, Q.; Wang, Y. SHRIMP zircon U-Pb age, litho- and biostratigraphic analyses of the Huaiyu Domain in South China–Evidence for a Neoproterozoic orogen, not Late Paleozoic-Early Mesozoic collision. *Episodes* **2006**, *29*, 244–252. [CrossRef]
51. Yu, J.-H.; Wang, L.; O'Reilly, S.Y.; Griffin, W.L.; Zhang, M.; Li, C.; Shu, L. A Paleoproterozoic orogeny recorded in a long-lived cratonic remnant (Wuyishan terrane), eastern Cathaysia Block, China. *Precambrian Res.* **2009**, *174*, 347–363. [CrossRef]
52. Yu, J.-H.; O'Reilly, S.Y.; Wang, L.; Griffin, W.L.; Zhou, M.-F.; Zhang, M.; Shu, L. Components and episodic growth of Precambrian crust in the Cathaysia Block, South China: Evidence from U–Pb ages and Hf isotopes of zircons in Neoproterozoic sediments. *Precambrian Res.* **2010**, *181*, 97–114. [CrossRef]
53. Li, L.M.; Min, S.; Wang, Y.; Xing, G.; Zhao, G.; Cai, K.; Zhang, Y. Geochronological and Geochemical study of Palaeoproterozoic gneissic granites and clinopyroxenite xenoliths from NW Fujian, SE China: Implications for the crustal evolution of the Cathaysia Block. *J. Asian Earth Sci.* **2011**, *41*, 204–212. [CrossRef]
54. Li, Z.X.; Li, X.H.; Zhou, H.W.; Kinny, P.D. Grenvillian continental collision in south China: New SHRIMP U–Pb zircon results and implications for the configuration of Rodinia. *Geology* **2002**, *30*, 163–166. [CrossRef]
55. Zhang, A.; Wang, Y.; Fan, W.; Zhang, Y.; Yang, J. Earliest Neoproterozoic (ca. 1.0 Ga) arc–back-arc basin nature along the northern Yunkai Domain of the Cathaysia Block: Geochronological and geochemical evidence from the metabasite. *Precambrian Res.* **2012**, *220–221*, 217–233. [CrossRef]
56. Gao, S.; Yang, J.; Zhou, L.; Li, M.; Hu, Z.; Guo, J.; Yuan, H.; Gong, H.; Xiao, G.; Wei, J. Age and growth of the Archean Kongling terrain, South China, with emphasis on 3.3 ga granitoid gneisses. *Am. J. Sci.* **2011**, *311*, 153–182. [CrossRef]
57. Soret, M.; Larson, K.P.; Cottle, J.; Ali, A. How Himalayan collision stems from subduction. *Geology* **2021**, *49*, 894–898. [CrossRef]
58. Qiu, Y.M.; Gao, S.; Macnaughton, N.J.; Ling, W.L. First evidence of ≥3.2Ga continental crust in the Yangtze craton of South China and its implications for Archean crustal evolution and Phanerozoic tectonics. *Geology* **2000**, *28*, 11–14. [CrossRef]
59. Gao, S.; Ling, W.L.; Qiu, Y.M.; Lian, Z.; Hartmann, G.; Simon, K. Contrasting geochemical and Sm-Nd isotopic compositions of Archean metasediments from the Kongling high-grade terrain of the Yangtze craton: Evidence for cratonic evolution and redistribution of REE during crustal anatexis. *Geochim. Cosmochim.* **1999**, *63*, 2071–2088. [CrossRef]
60. Zong, K.; Klemd, R.; Yuan, Y.; He, Z.; Guo, J.; Shi, X.; Liu, Y.; Hu, Z.; Zhang, Z. The assembly of Rodinia: The correlation of early Neoproterozoic (ca. 900 Ma) high-grade metamorphism and continental arc formation in the southern Beishan Orogen, southern Central Asian Orogenic Belt (CAOB). *Precambrian Res.* **2017**, *290*, 32–48. [CrossRef]
61. Liu, Y.; Gao, S.; Hu, Z.; Gao, C.; Zong, K.; Wang, D. Continental and Oceanic Crust Recycling-induced Melt-Peridotite Interactions in the Trans-North China Orogen: U-Pb Dating, Hf Isotopes and Trace Elements in Zircons from Mantle Xenoliths. *J. Petrol.* **2010**, *51*, 537–571. [CrossRef]
62. Ludwing, K.R. Users Manual for IsoplotEx 3.75: A geochronological toolkit for Microsoft Excel. *Berkeley Geochronol. Cent. Spec. Publ.* **2012**, *5*, 1–75.
63. Liu, Y.; Zong, K.; Kelemen, P.B.; Gao, S. Geochemistry and magmatic history of eclogites and ultramafic rocks from the Chinese continental scientific drill hole: Subduction and ultrahigh-pressure metamorphism of lower crustal cumulates. *Chem. Geol.* **2008**, *247*, 133–153. [CrossRef]
64. Hu, Z.; Liu, Y.; Gao, S.; Xiao, S.; Zhao, L.; Günther, D.; Li, M.; Zhang, W.; Zong, K. A "wire" signal smoothing device for laser ablation inductively coupled plasma mass spectrometry analysis. *Spectrochim. Acta Part B At. Spectrosc.* **2012**, *78*, 50–57. [CrossRef]
65. Hu, Z.; Gao, S.; Liu, Y.; Chen, H.; Hu, S. Accurate Determination of Rare Earth Elements in USGS, NIST SRM, and MPI-DING Glasses by Excimer LA-ICP-MS at High Spatial Resolution. *Spectrosc. Lett.* **2008**, *41*, 228–236. [CrossRef]
66. Hu, Z.; Liu, Y.; Gao, S.; Liu, W.; Zhang, W.; Tong, X.; Lin, L.; Zong, K.; Li, M.; Chen, H.; et al. Improved in situ Hf isotope ratio analysis of zircon using newly designed X skimmer cone and jet sample cone in combination with the addition of nitrogen by laser ablation multiple collector ICP-MS. *J. Anal. At. Spectrom.* **2012**, *27*, 1391–1399. [CrossRef]
67. Hoskin, P.W.; Schaltegger, U. The Composition of Zircon and Igneous and Metamorphic Petrogenesis. *Rev. Mineral. Geochem.* **2003**, *53*, 27–62. [CrossRef]
68. Le Maitre, R.W. Chemical variability of some common igneous rocks. *J. Petrol.* **1976**, *17*, 589–637. [CrossRef]
69. Peccerillo, A.; Taylor, S.R. Geochemistry of Eocene Calc-Alkaline Volcanic Rocks from the Kastamonu Area, Northern Turkey. *Contrib. Mineral. Petrol.* **1976**, *58*, 63–81. [CrossRef]
70. Maniar, P.D.; Piccoli, P.M. Tectonic discrimination of granitoids. *Geol. Soc. Am. Bull.* **1989**, *101*, 635–643. [CrossRef]
71. Rudnick, R.L.; Gao, S. *The Composition of the Continental Crust*; Elsevier: Amsterdam, The Netherlands, 2003; Volume 3.
72. Li, Y.; He, H.; Wang, C.; Wei, Y.; Chen, X.; He, J.; Ning, Z.; Zhou, A. Early Cretaceous (ca. 100 Ma) magmatism in the southern Qiangtang subterrane, central Tibet: Product of slab break-off? *Int. J. Earth Sci.* **2016**, *106*, 1289–1310. [CrossRef]
73. Whalen, J.B.; Currie, K.L.; Chappell, B.W. A-type granites geochemiclcharacterist discrimination and petrogenes. *Contrib. Mineral. Petrol.* **1987**, *95*, 407–419. [CrossRef]
74. Chappell, B.W.; White, A.J.R. Two contrasting granite types. *Pac. Geol.* **1974**, *8*, 173–174. [CrossRef]
75. Sylvester, P.J. Post-Collisional Alkaline Granites. *J. Geol.* **1989**, *97*, 261–280. [CrossRef]
76. Harris, N.B.W.; Pearce, J.A.; Tindle, A.G. *Geochemical Characteristics of Collision-Zone Magmatism*; Geological Society: London, UK, 1986; Volume 19.

77. Li, X.H.; Li, Z.X.; Li, W.X.; Liu, Y.; Yuan, C.; Wei, G.J.; Qi, C.S. U–Pb zircon, geochemical and Sr–Nd–Hf isotopic constraints on age and origin of Jurassic I- and A-type granites from central Guangdong, SE China: A major igneous event in response to foundering of a subducted flat-slab? *Lithos* **2007**, *96*, 186–204. [CrossRef]
78. Chappell, B.W.; Stephens, W.E. Origin of infracrustal (I-type) granite magmas. *Trans. R. Soc. Edinb. Earth Sci.* **1988**, *79*, 71–86. [CrossRef]
79. Sisson, T.W.; Ratajeski, K.; Hankins, W.B.; Glazner, A.F. Voluminous granitic magmas from common basaltic sources. *Contrib. Mineral. Petrol.* **2005**, *148*, 635–661. [CrossRef]
80. Topuz, G.; Altherr, R.; Siebel, W.; Schwarz, W.H.; Zack, T.; Hasözbek, A.; Barth, M.; Satır, M.; Şen, C. Carboniferous high-potassium I-type granitoid magmatism in the Eastern Pontides: The Gümüşhane pluton (NE Turkey). *Lithos* **2010**, *116*, 92–110. [CrossRef]
81. Chen, B.; Arakawa, Y. Elemental and Nd-Sr isotopic geochemistry of granitoids from the West Junggar foldbelt (NW China), with implications for Phanerozoic continental growth. *Geochim. Cosmochim. Acta* **2005**, *69*, 1307–1320. [CrossRef]
82. DePaolo, D.J. Trace element and isotopic effects of combined wallrock assimilation and fractional crystallization. *Earth Planet. Sci. Lett.* **1981**, *53*, 189–202. [CrossRef]
83. Zhang, D.H.; Wei, J.H.; Fu, L.B.; Chen, H.Y.; Tan, J.; Li, Y.J.; Shi, W.J.; Tian, N. Formation of the Jurassic Changboshan-Xieniqishan highly fractionated I-type granites, northeastern China: Implication for the partial melting of juvenile crust induced by asthenospheric mantle upwelling. *Geol. J.* **2015**, *50*, 122–138. [CrossRef]
84. Hu, P.Y.; Li, C.; Li, J.; Wang, M.; Xie, C.M.; Wu, Y.W. Zircon U–Pb–Hf isotopes and whole-rock geochemistry of gneissic granites from the Jitang complex in Leiwuqi area, eastern Tibet, China: Record of the closure of the Paleo-Tethys Ocean. *Tectonophysics* **2014**, *623*, 83–99. [CrossRef]
85. Zhu, R.-Z.; Lai, S.-C.; Qin, J.-F.; Zhao, S.-W. Early-Cretaceous highly fractionated I-type granites from the northern Tengchong block, western Yunnan, SW China: Petrogenesis and tectonic implications. *J. Asian Earth Sci.* **2015**, *100*, 145–163. [CrossRef]
86. He, H.Y.; Li, Y.L.; Wang, C.S.; Han, Z.P.; Ma, P.F.; Xiao, S.Q. Petrogenesis and tectonic implications of Late Cretaceous highly fractionated I − type granites from the Qiangtang block, central Tibet. *J. Asian Earth Sci.* **2019**, *176*, 337–352. [CrossRef]
87. Yang, J.H.; Sun, J.F.; Zhang, J.H.; Wilde, S.A. Petrogenesis of Late Triassic intrusive rocks in the northern Liaodong Peninsula related to decratonization of the North China Craton: Zircon U–Pb age and Hf–O isotope evidence. *Lithos* **2012**, *153*, 108–128. [CrossRef]
88. Clemens, J.D.; Darbyshire, D.P.F.; Flinders, J. Sources of post-orogenic calcalkaline magmas: The Arrochar and Garabal Hill–Glen Fyne complexes, Scotland. *Lithos* **2009**, *112*, 524–542. [CrossRef]
89. Chen, J.L.; Xu, J.F.; Yu, H.X.; Wang, B.D.; Wu, J.B.; Feng, Y.F. Late Cretaceous high-Mg# granitoids in southern Tibet: Implications for the early crustal thickening and tectonic evolution of the Tibetan Plateau? *Lithos* **2015**, *232*, 12–22. [CrossRef]
90. Zhu, D.C.; Mo, X.X.; Wang, L.Q.; Zhao, Z.D.; Niu, Y.L.; Zhou, C.Y.; Yang, Y.H. Petrogenesis of highly fractionated I-type granites in the Chayu area of eastern Gangdese, Tibet: Constraints from zircon U-Pb geochronology, geochemistry and Sr-Nd-Hf isotopes. *Sci. China Serise D-Earth Sci.* **2009**, *39*, 833–848.
91. Kemp, A.I.S.; Hawkesworth, C.J.; Fostern, G.L.; Paterson, B.A.; Woodhead, J.D.; Hergt, J.M.; Gray, C.M.; Whitehouse, M.J. Magmatic and crustal differentiation history of granitic rocks from Hf-O isotopes in zircon. *Science* **2007**, *315*, 980–983. [CrossRef]
92. Bolhar, R.; Weaver, S.D.; Whitehouse, M.J.; Palin, J.M.; Woodhead, J.D.; Cole, J.W. Sources and evolution of arc magmas inferred from coupled O and Hf isotope systematics of plutonic zircons from the Cretaceous Separation Point Suite (New Zealand). *Earth Planet. Sci. Lett.* **2008**, *268*, 312–324. [CrossRef]
93. Belousova, E.A.; Griffin, W.L.; O'Reilly, S.Y. Zircon Crystal Morphology, Trace Element Signatures and Hf Isotope Composition as a Tool for Petrogenetic Modelling: Examples from Eastern Australian Granitoids. *J. Petrol.* **2006**, *47*, 329–353. [CrossRef]
94. Griffin, W.L.; Wang, X.; Jackson, S.E.; Perace, N.J.; O'Reilly, S.Y.; Xu, X.S.; Zhou, X.M. Zircon chemistry and magma mixing, SE China: In-situ analysis of Hf isotopes, Tonglu and Pingtan igneous complexes. *Lithos* **2002**, *61*, 237–269. [CrossRef]
95. Benoit, M.; Aguillón-Robles, A.; Calmus, T.; Maury, R.C.; Bellon, H.; Cotten, J.; Bourgois, J.; Michaud, F. Geochemical Diversity of Late Miocene Volcanism in Southern Baja California, Mexico: Implication of Mantle and Crustal Sources during the Opening of an Asthenospheric Window. *J. Geol.* **2002**, *110*, 627–648. [CrossRef]
96. Ickert, R.B.; Thorkelson, D.J.; Marshall, D.D.; Ullrich, T.D. Eocene adakitic volcanism in southern British Columbia: Remelting of arc basalt above a slab window. *Tectonophysics* **2009**, *464*, 164–185. [CrossRef]
97. Wu, F.Y.; Li, X.H.; Zheng, Y.F.; Gao, S. Lu-Hf isotopic systematics and their applications in petrology. *Acta Petrol. Sin.* **2007**, *23*, 185–220.
98. Yang, Q.K.; Hua, C.; Yu, Y.S.; Zhang, X.L. Genesis of Caledonian granodiorite in Nancheng, central Jiangxi: Constraints from LA-ICP-MS zircon U–Pb geochronology and geochemistry. *J. Guilin Univ. Technol.* **2019**, *39*, 781–792.
99. Zong, Z.-J.; Du, Y.-S.; Li, S.-T.; Cao, Y.; Du, J.-G.; Deng, X.-H.; Xue, L.-W. Petrogenesis of the early Permian A-type granites in the Halajun region, southwest Tianshan, western Xinjiang, NW China: Implications for geodynamics of Tarim large igneous province. *Int. Geol. Rev.* **2020**, *63*, 1110–1131. [CrossRef]
100. Wang, Y.; Fan, W.; Zhang, G.; Zhang, Y. Phanerozoic tectonics of the South China Block: Key observations and controversies. *Gondwana Res.* **2013**, *23*, 1273–1305. [CrossRef]
101. Wang, Y.; Zhang, A.; Fan, W.; Zhang, Y.; Zhang, Y. Origin of paleosubduction-modified mantle for Silurian gabbro in the Cathaysia Block: Geochronological and geochemical evidence. *Lithos* **2013**, *160–161*, 37–54. [CrossRef]

102. Shu, L.-S.; Faure, M.; Yu, J.-H.; Jahn, B.-M. Geochronological and geochemical features of the Cathaysia block (South China): New evidence for the Neoproterozoic breakup of Rodinia. *Precambrian Res.* **2011**, *187*, 263–276. [CrossRef]
103. Li, Z.X.; Li, X.H.; Kinny, P.D.; Wang, J. The breakup of Rodinia: Did it start with a mantle plume beneath South China? *Earth Planet. Sci. Lett.* **1999**, *173*, 171–181. [CrossRef]
104. Wang, X.-C.; Li, X.-H.; Li, W.-X.; Li, Z.-X. Variable involvements of mantle plumes in the genesis of mid-Neoproterozoic basaltic rocks in South China: A review. *Gondwana Res.* **2009**, *15*, 381–395. [CrossRef]
105. Hsü, K.J.; Li, J.L.; Chen, H.H.; Wang, Q.C.; Sun, S.; Sengor, A.M.C. Tectonics of South China: Key to understanding West Pacific WMY. *Tectonophysics* **1990**, *183*, 9–39. [CrossRef]
106. Guo, L.Z.; Shi, Y.S.; Lu, H.F.; Ma, R.S.; Dong, H.G.; Yang, S.F. The pre-Devonian tectonic patterns and evolution of South China. *J. Southeast Asian Earth Sci.* **1989**, *3*, 87–93.
107. Shui, T. Tectonic framework of the southeastern China continental basement. *Sci. China Ser.B* **1988**, *31*, 414–421.
108. Li, L.-M.; Sun, M.; Wang, Y.; Xing, G.; Zhao, G.; Lin, S.; Xia, X.; Chan, L.; Zhang, F.; Wong, J. U–Pb and Hf isotopic study of zircons from migmatised amphibolites in the Cathaysia Block: Implications for the early Paleozoic peak tectonothermal event in Southeastern China. *Gondwana Res.* **2011**, *19*, 191–201. [CrossRef]
109. Wang, Y.; Zhang, F.; Fan, W.; Zhang, G.; Chen, S.; Cawood, P.A.; Zhang, A. Tectonic setting of the South China Block in the early Paleozoic: Resolving intracontinental and ocean closure models from detrital zircon U-Pb geochronology. *Tectonics* **2010**, *29*, 1–16. [CrossRef]
110. Charvet, J.; Shu, L.; Faure, M.; Choulet, F.; Wang, B.; Lu, H.; Breton, N.L. Structural development of the Lower Paleozoic belt of South China: Genesis of an intracontinental orogen. *J. Asian Earth Sci.* **2010**, *39*, 309–330. [CrossRef]
111. Jiayu, R.; Junxuan, F.; Miller, A.I.; Guoxiang, L. Dynamic patterns of latest Proterozoic-Palaeozoic-early Mesozoic marine biodiversity in South China. *Geol. J.* **2007**, *42*, 431–454. [CrossRef]
112. Chen, X.; Rong, J.Y.; Charles, E.M.; David, A.T.H.; Zhang, R.B.; Zhang, R.D.; Li, R.Y.; Wang, Y. Late Ordovician to earliest Silurian graptolite and brachiopod biozonation from the Yangtze region, South China, with a global correlation. *Geol. Mag.* **2000**, *137*, 623–650. [CrossRef]
113. Yan, D.-P.; Zhou, M.-F.; Wang, C.Y.; Xia, B. Structural and geochronological constraints on the tectonic evolution of the Dulong-Song Chay tectonic dome in Yunnan province, SW China. *J. Asian Earth Sci.* **2006**, *28*, 332–353. [CrossRef]
114. Pearce, J.A.; Harris, N.B.W.; Tindle, A.G. Trace Element Discrimination Diagrams for the Tectonic Interpretation of Granitic Rocks. *J. Petrol.* **1984**, *25*, 956–983. [CrossRef]
115. England, P.C.; Thompson, A.B. Pressure–temperature–time paths of regions metamorphism I. Heat transfer during the evolution of regions of thickened continental crust. *J. Petrol.* **1984**, *25*, 894–928. [CrossRef]
116. Turner, S.; Sandiford, M.; Foden, J. Some geodynamic and compositional constraints on "postorogenic" magmatism. *Geology* **1992**, *20*, 931. [CrossRef]
117. Gutiérrez-Alonso, G.; Murphy, B.; Fernández-Suárez, J.; Weil, A.B.; Franco, M.P.; Gonzalo, J.C. Lithospheric delamination in the core of Pangea: Sm–Nd insights from the Iberian mantle. *Geology* **2011**, *39*, 155–158. [CrossRef]
118. Gvirtzman, Z. Partial detachment of a lithospheric root under the southeast Carpathians: Toward a better definition of the detachment concept. *Geology* **2002**, *30*, 51–54. [CrossRef]
119. Wang, X.-L.; Zhou, J.-C.; Wan, Y.-S.; Kitajima, K.; Wang, D.; Bonamici, C.; Qiu, J.-S.; Sun, T. Magmatic evolution and crustal recycling for Neoproterozoic strongly peraluminous granitoids from southern China: Hf and O isotopes in zircon. *Earth Planet. Sci. Lett.* **2013**, *366*, 71–82. [CrossRef]